ICAS 2020 SHANGHAI
International Council of the Aeronautical Sciences
32nd Congress of the International Council of the Aeronautical Sciences
September 6-10, 2021
Pudong Shangri-La, Shanghai, China

EXPERIMENTAL VALIDATION OF NUMERICAL PREDICTION OF WING-PROPELLER AERODYNAMIC INTERACTION

Sergio De Lucas-Bodas[1]; Jorge Narbona-Gonzalez[1]; Victor Ossorio-Contreras[1]; Juan José Guerra-Crespo[1]; David E. Funes-Sebastian[1]; Luis P. Ruiz-Calavera[2]

[1]Airbus Defence & Space, Aerodynamics Domain, Getafe, Spain
[2]Airbus Defence & Space, Flight Physics CoC, Getafe, Spain

Abstract

The mutual aerodynamic interaction between the wing and the propeller is described. Propeller driven aircrafts interest is increasing nowadays and the correct propeller integration can lead to significant aerodynamics improvements or affecting the project feasibility if this interaction is not well captured. The wing-propeller interaction problem is still difficult to predict by CFD in its complete extension. The paper introduces those effects by means of wind tunnel test results and compares the accuracy of two CFD methodologies.

Keywords: Aerodynamics, Propeller, CFD, Wind Tunnel Test

1. Introduction

In order to reduce the environmental footprint of the aviation sector, significant efforts are being devoted in the search of alternative propulsive systems, such as electric-based or hydrogen-based, and as a consequence this is leading to an increased interest in propeller driven aircraft configurations. The *EcoPulse* demonstrator [1] developed by Daher, Safran and Airbus and the *Zeroe* Airbus program [2] are both examples of the new trend.

Correct propeller integration within the aircraft is critical as it can lead to significant aerodynamics improvements increasing the aircraft efficiency, especially when propulsion is well distributed along the wing span as it is stated by Dae Kim [3] and Stoll et al [4], or even affecting the feasibility of the aircraft project in case this integration is not well implemented. This integration is not an easy process, especially in non-conventional configurations, as the mutual aerodynamic interaction between the wing and the propeller is a problem which is still difficult to predict by CFD in its complete extension, particularly for closely coupled wing-propeller configurations, multiple propellers in close proximity, over-the-wing propellers, tip wing propellers, etc. Despite those difficulties related with the CFD simulations, the truth is that including wing-propeller interaction in the preliminary phases of the design will improve final aircraft performances as well as avoid unexpected behavior.

During the design phase the effect of the propeller slipstream on the aircraft aerodynamic characteristics (the so-called indirect power-effects) must be correctly predicted for the different flap configurations or relative propeller-wing positions. But also the impact of the wing, or the nearby propellers, on the propeller efficiency and the associated loads needs to be properly captured from the early conceptual design stages. In particular the prediction of propeller in-plane loads (the so-called 1P forces and moments) remains a difficult problem, and one that is very important because in addition to the impact of these loads on aircraft stability they also significantly contribute to the design loads of the wing, the gearbox, engine shaft and the engine mounting system.

The starting point in this direction is to have the capability to predict these effects in a conventional propeller installation configuration. To these aim a series of wind tunnel tests have been performed in June 2019 on a low speed wind tunnel (the RUAG LWTE [5]) of a model of the C295W aircraft within the European project Clean Sky 2, CS2 hereafter. Experimental data has been gathered in terms of global aerodynamic coefficients, thrust, torque, 1P forces and 1P moments on each propeller, and flow visualizations.

In addition, an extensive Computation Fluid Dynamics (CFD) campaign was conducted to compare the predictions with the experimental data as well as validating the results. Along section 5 a set of those CFD evaluations will be compared with wind tunnel test results presented in section 4.

2. Aircraft-Propeller Interaction

As it was anticipated in section 1 in the aircraft-propeller bi-directional interaction there are several effects, which will be described hereafter. Those effects will be divided into two different sets, the influence of aircraft setting and attitude on the propeller performance, and the influence of the propeller in the aircraft loads, stability and performance due to either the proper propeller loads or the indirect effects of the propeller slipstream.

2.1 Aircraft Effects on Propellers

Let us define the inflow as the relative direction of the fluid in the propeller inlet referred to the propeller plane. Thus, the main responsible of the propeller inflow is the aircraft attitude; however, it is modified due to the presence of those components of the aircraft close to or upstream of the propeller. In the same way that the aircraft forward fuselage modifies the fluid over the wing and the wing modifies the fluid conditions at tail location, the inflow will be affected by any aircraft component, for example, tail mounted propellers are influenced by the wing downwash.

In addition, the inflow will be also be affected by those components of the aircraft which, without being upstream of the proper propeller, are close enough to modify their neighborhood. That is the case of the wing controls, such as flap deflection, ailerons, slats or spoilers, which influence wing mounted propellers. Any change on these devices will modify the induced angles distribution along the span directly affecting the propeller inflow.

The correct modelling of this effect is imperative to properly estimate propeller efficiency, propeller loads – which size gearbox, engine shaft, engine mounting system and wing –, as well as the indirect power-effects described hereafter.

2.2 Propeller Effects on Aircraft

Once the effects of the aircraft on the propeller have been described, we must focus on the opposite, the effects that the propeller, both direct and indirect, cause on the aircraft loads, performance and stability. At first it is to be said that the propeller is designed in order to generate thrust by minimizing the torque. The thrust is the force normal to the propeller plane that allows sustained flight, while the torque is the moment normal to the propeller plane that the engines must overcome to achieve the desired thrust.

In the ideal case in which the flow at the propeller plane is axial-symmetric, the propeller would only generate forces and moments normal to the propeller plane, thrust and torque; the other components of the force and moment would be identically null. However, the local fluid direction is rarely normal to the propeller plane; as a consequence, blade thrust and tangential forces are not axial-symmetric, and this generates in-plane forces and moments in the complete propeller, the so-called 1P-loads. These loads significantly contribute to both the aircraft stability and the design loads.

The last effect is related with the propeller wake impingement on the aircraft surface. The propeller operation will induce a dynamic pressure increment which increases lift and drag of the impinged surfaces. In addition, the rotation of the propeller generates certain amount of swirl, which modifies the distribution of angles of attack and sideslip downstream.

In case of wing mounted propellers, the propeller wake alters the wing lift distribution, modifying wing loads, induced drag and even wing stall behavior. Furthermore, the wing downwash is also significantly affected, eventually modifying the tail performance. These effects are of paramount importance in propeller aircraft design.

3. Case Study

The selected case to carry out the analysis is encompassed within the CS2 project which main objective is related with the reduction of fuel consumption. In fact the Airbus D&S C295W [6] based CS2 FTB2 prototype is focused on the combination of conventional control devices in order to improve aerodynamic efficiency, increase maneuverability and reduce the structure weight by modifying the wing load distribution during maneuvers or in the presence of gusts.

Particularly, the FTB2 prototype features a continuous flap deployment which allows, in conjunction with the spoilers, aileron and winglet-tab deflections, to optimize aircraft performance for different operations. As it can be extracted from previous sections, the performance of these elements is highly influenced by the propeller operation.

Furthermore, CS2 FTB2 flap might be set either as a single slotted or as a double slotted flap. This feature will be used to analyze propeller-flap interaction on both kinds of flaps.

The figure below corresponds with the FTB2 prototype; note that the flaps are located immediately behind the propellers; thus, their wakes directly affect the flap performance.

Figure 1 – CS2 FTB2 prototype

4. Wind Tunnel Tests

4.1 Wind Tunnel Test Description

The POLITE (Powered, modular Wind-Tunnel model for low and high Reynolds tests) model is a 1:8.6 scaled wind tunnel model representing the FTB2 demonstrator configuration, in the frame of Clean Sky 2 initiative (see Figure 2). This model is designed and manufactured by the POLITE consortium which is formed by IBK, ARA, RUAG and Dream.

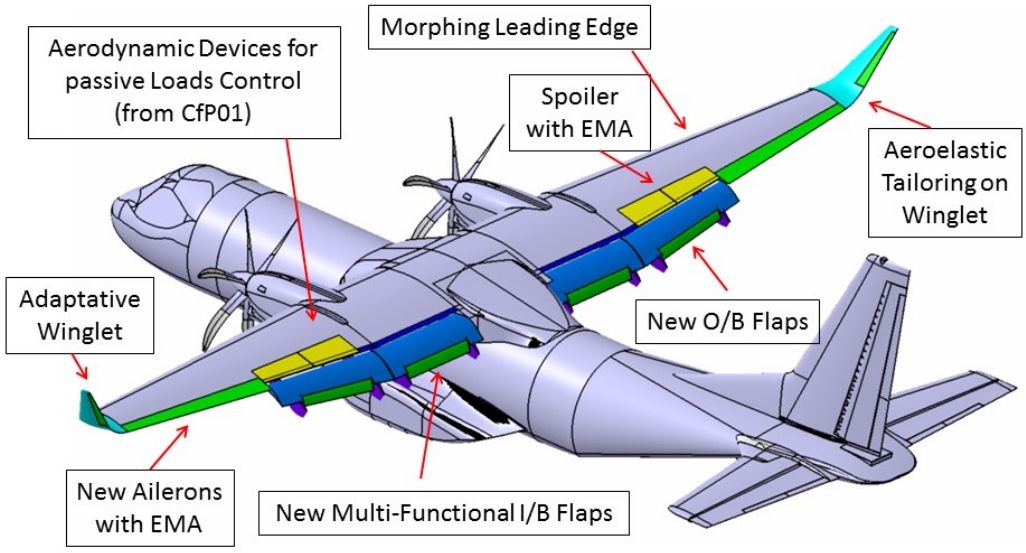

Figure 2 - Overview of FTB2 main features

The model was designed and manufactured with the objective of being able to be tested at both low and high Reynolds numbers facilities, with the maximum possible commonality in the model parts between both facilities. This means that the model is able to withstand stresses related to pressurized wind tunnel facilities and the power system of the engines can provide a large amount of power.

Also, thanks to its modularity, the model is able to be tested both in power-on and power-off configurations, tails on and off, with different values of horizontal and vertical tail planes setting angles and different control deflections, including flaps, ailerons, spoilers, winglet tabs, elevators and rudder.

Apart from global loads measured by a main balance, propeller blades are instrumented with strain gauges to monitor their structural health. Also, the model is equipped with local balances in the propeller hubs to measure propeller loads (6-DOF rotary shaft balances with telemetry data acquisition), as well as pressure taps required to correct the back pressure of the RSBs. These elements allow separating the direct propeller effects from the main balance measurements, thus obtaining the indirect propeller effects on the aircraft.

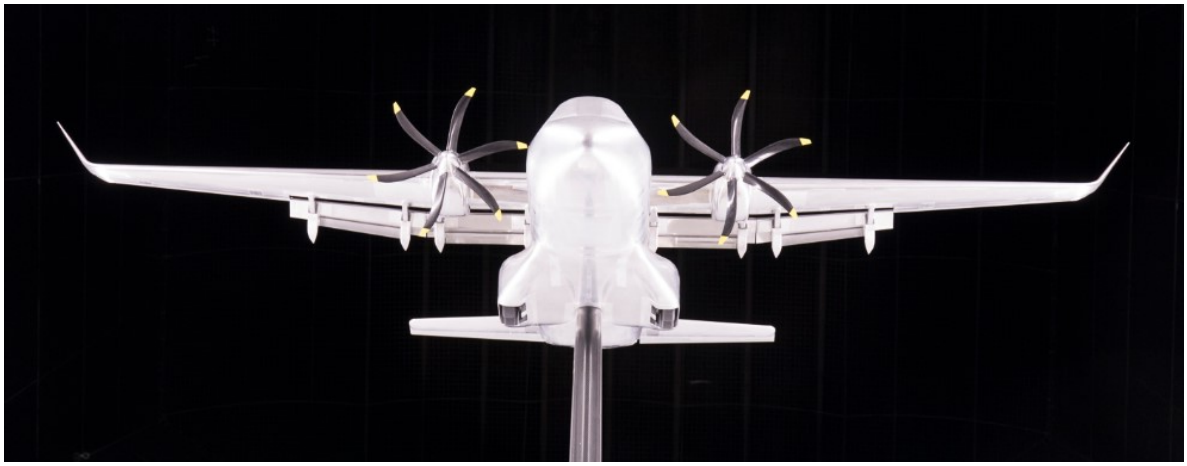

Figure 3 – POLITE Model

The low Reynolds wind tunnel tests were performed at RUAG's Large Wind Tunnel Emmen (RUAG-LWTE), which is an atmospheric, low speed, closed-circuit wind tunnel located at Emmen, Switzerland. This wind tunnel has a test section of 7x5 squared meters and can reach an airspeed up to Mach 0.2.

The tests performed at RUAG were devoted to data gathering for aero-dataset generation, including:

- Characterization of the tails-off configuration, including different flap configurations and power effects
- Tail characterization, including elevator and rudder control power at power-off and power-on, at different flap configurations
- Full characterization of the new FTB2 aerodynamic devices (ailerons, spoilers, winglet tabs, flap performances…)
- Aerodynamic efficiency optimization using ailerons and winglet tabs
- Drag measurements
- Characterization of the downwash and sidewash at tail location, at different flap configurations, with and without propeller effects, as well as characterization of the dynamic pressure ratio at tail location
- Analysis of the tail stall
- Failure cases

4.2 Results

Along this section some of those results obtained in the wind tunnel test campaign described above will be presented. Wind tunnel test results will be presented comparing the power-off (without propellers) and the power-on (with propellers) aircraft in order to evaluate the influence of the propeller operation in the global coefficients.

Attending the wind tunnel test conditions, the Mach number (M) is equal to 0.15 while the Reynolds number per length unit (Re/c) is equal to $3.5 \cdot 10^6$. Single and double slotted flap settings have been selected in order to show the propeller-aircraft interaction described in section 2.

As it was already anticipated, we are focusing our study on the indirect effects of the propeller in the lift and pitching moment global coefficients and on the propeller direct effects, particularly on the in-plane loads.

4.2.1 Global Coefficients

Let us focus on longitudinal coefficients lift and pitch, namely CL and CD in order to illustrate the main propeller effects on global coefficients. Let us define CLref and CDref as

$$CLref = CL^{Poff}\ (\alpha = 0), \text{and} \qquad Cmref = Cm^{Poff}\ (\alpha = 0), \tag{1}$$

where α is the aircraft angle of attack. These coefficients will be used as reference in figures below due to confidential issues.

As it can be observed in Figure 4, the lift coefficient is highly influenced by the operation of the propeller. Its wake causes an increase in local lift due to the dynamic pressure increment which not only increases the lift coefficient but also delays the stall angle.

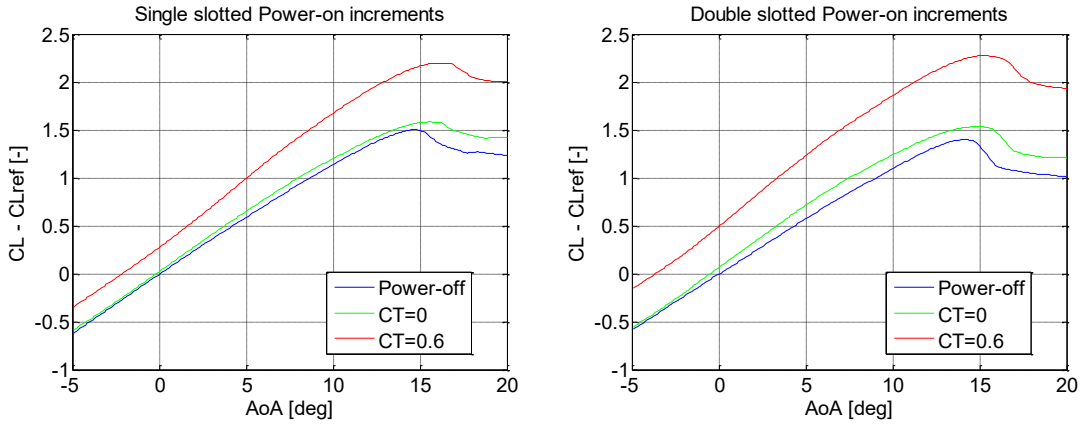

Figure 4 - Lift coefficient at power-off (blue), CT=0 (green) and CT=0.6 (red) for single slotted flap (left) and double slotted flap (right).

In addition, it can be observed that power on lift increment is greater in the double slotted flap, as the power-off lift coefficient is also greater. Propeller effects on lift at CT=0.6 are pictured in Figure 5 for both flaps. Note, that CT is the non-dimensional thrust obtained as

$$CT = \frac{T}{\frac{1}{2}\rho V^2 S} \tag{2}$$

where, ρ is the air density at wind tunnel conditions, V is the wind velocity and S is the wind tunnel model surface.

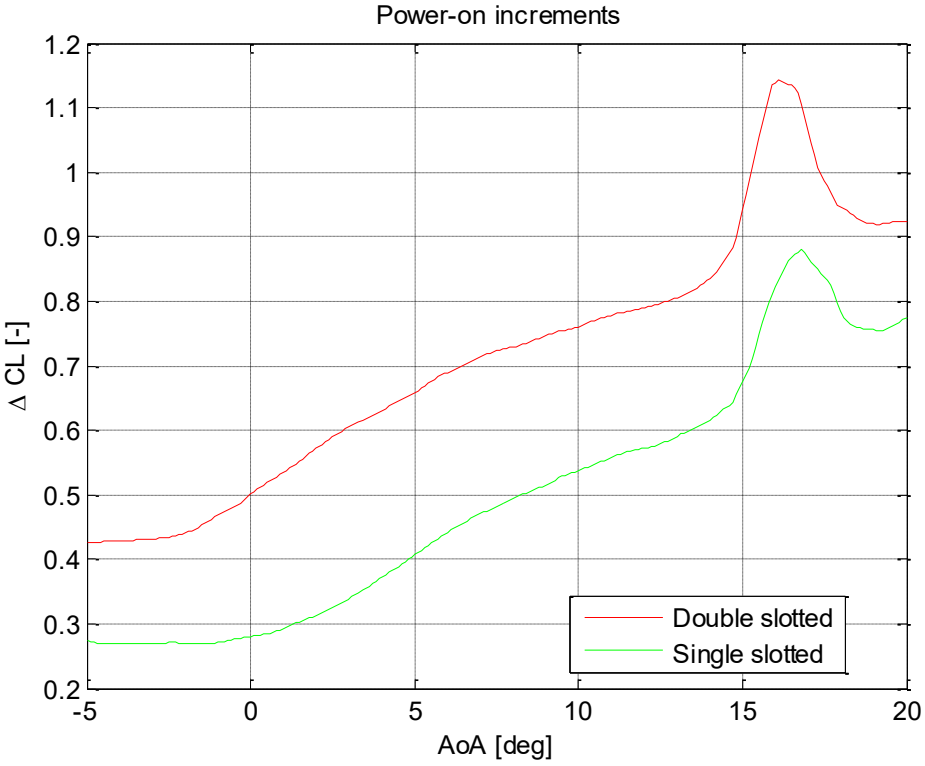

Figure 5 - Lift coefficient increment due to propeller operation (CT=0.6). Single slotted flap (green) and double slotted flap (red).

Considering these results, we can confirm the high interaction between the propeller and its neighborhood due to the propeller wake. Its effect on the lift coefficient is a function of both the propeller thrust and the lift at power-off conditions, which is related to the flap and control settings downstream of the propeller. Despite this conclusion is well known it reinforces the necessity of correctly predicting the propeller effects in early design phases. Note that the magnitude of ΔCL is remarkable.

The increment of the dynamic pressure in the propeller wake can also affect the tail lift, thus modifying aircraft stability. This effect might be seen as beneficial, since the greater dynamic pressure increment increases the tail lift derivative with the angle of attack as well as the elevator control power. However, there actually is a non-desirable effect related with the wing lift increment: a stronger wing downwash which reduces the local angle of attack at tail location.

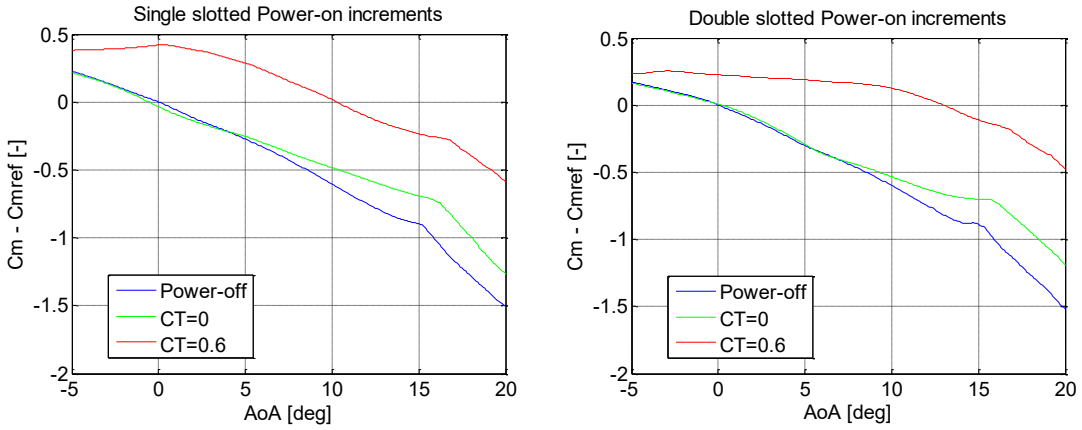

Figure 6 - Pitch coefficient at power-off (blue), CT=0 (green) and CT=0.6 (red) for single slotted flap

Analyzing the data in Figure 6, it can be observed that, even if the thrust coefficient is equal to zero, the aircraft pitching coefficient derivative with angle of attack is less negative. This effect is directly related with the downwash derivative increment, which becomes more relevant as the thrust coefficient rises.

(left) and double slotted flap (right).

4.2.2 In Plane Loads

Once the effects of the propeller blowing on the aircraft have been introduced in previous section we are focusing now in the loads appearing in the propeller due to its proper operation. The projection of the blade's force and moment into its plane are known as in-plane or 1P loads. Let us define the components or these loads, which are referred to the propeller center.

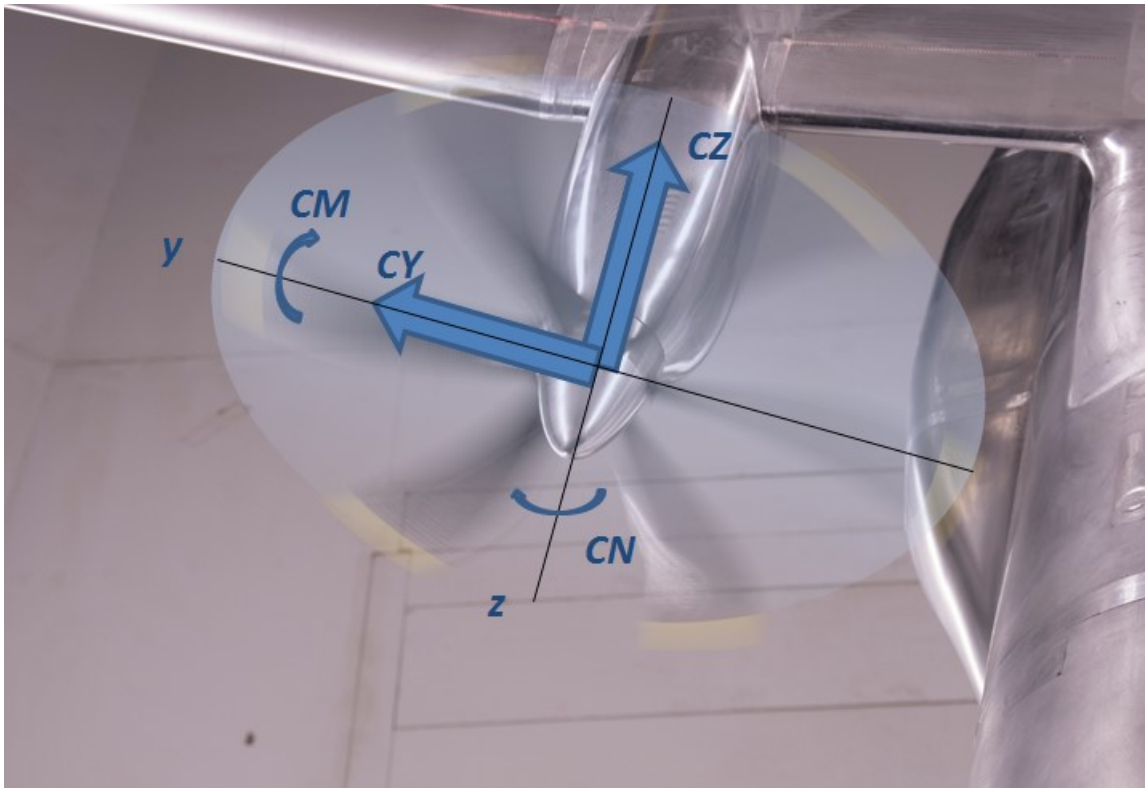

Figure 7 - Starboard propeller forces

The projections of 1P forces into the propeller plane is decomposed into lateral and vertical loads, forces and moments, noted as CY, CZ, CM and CN which are schematized in Figure 7. Those coefficient are obtained as

$$CY = \frac{Y}{\frac{1}{2}\rho V^2 S}, CZ = \frac{Z}{\frac{1}{2}\rho V^2 S}, CM = \frac{M}{\frac{1}{2}\rho V^2 S l_a}, and \;\; CN = \frac{N}{\frac{1}{2}\rho V^2 S l_a} \tag{3}$$

where l_a is the wind tunnel model mean aerodynamic chord and Y, Z, M and N are the measures of the rotatory shaft balances.

In Figure 8 the vertical 1P forces measured in the wind tunnel tests are depicted. As it was expected those loads depend mainly on the thrust coefficient; however, as it is aforementioned there is a

second order dependence with the aircraft configuration, as it can be extracted from Figure 8, increasing the 1P loads as it does the local lift coefficient; thus, double slotted flap generates slightly greater values of those in-plane loads.

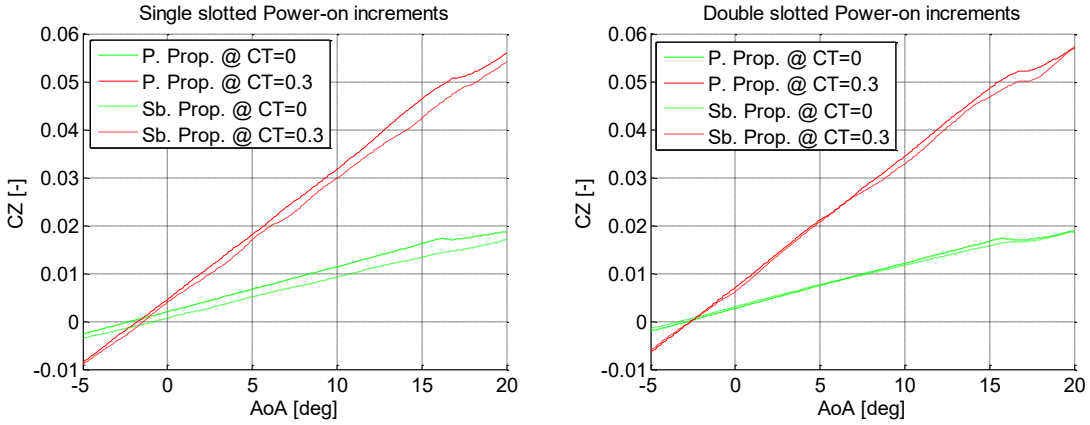

Figure 8 – 1P vertical force on the port and starboard propellers (CZ). Single slotted flap (left) and double slotted flap (right)

Note that, this vertical force will induce longitudinal instability if the propeller is positioned upstream of the aircraft gravity center which should be joined to the proper 1P pitching moment illustrated in Figure 9.

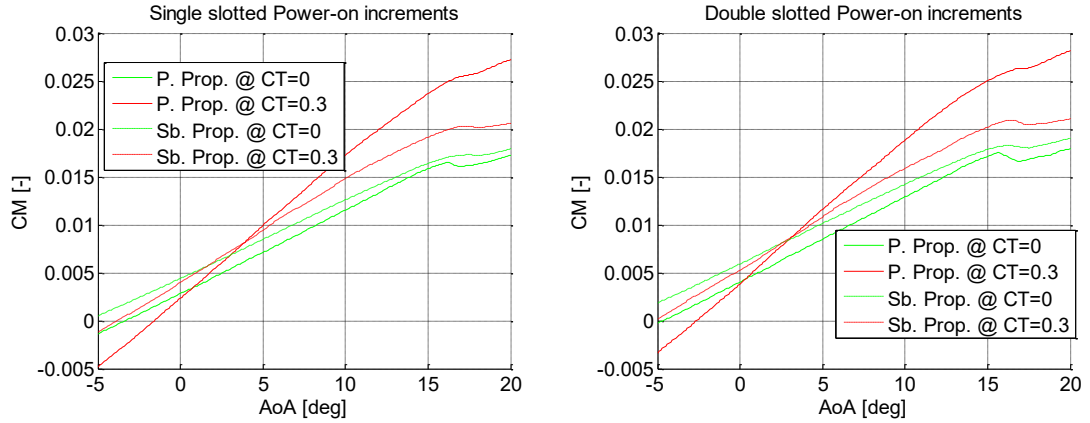

Figure 9 – 1P pitching moment on the port and starboard propellers (CM). Single slotted flap (left) and double slotted flap (right)

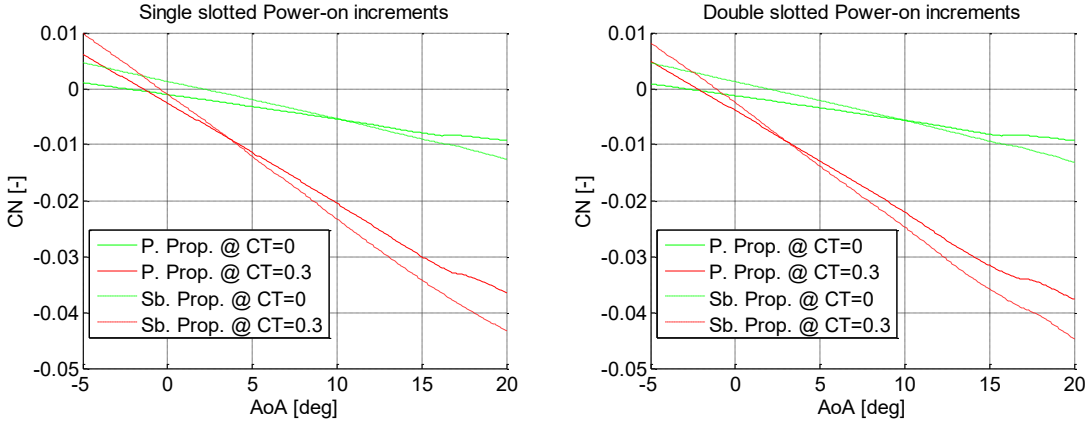

Figure 10 – 1P yawing moment on the port and starboard propellers (CN). Single slotted flap (left) and double slotted flap (right)

Finally, the propeller 1P yawing moment (CN) is also included in Figure 10 due to its high dependence with the angle of attack while the lateral force dependence is negligible.

4.2.3 Visualizations

In order to complete and illustrate some of the aforementioned observations, a set of wind tunnel test visualizations are shown in this section. In these visualizations the fluid streamlines over the wing and horizontal tail plane (HTP) surfaces are visible.

In Figure 11 and Figure 12, the streamlines over the wing surface at single and double slotted flap respectively are shown at CT=0 & near the aircraft stall. These visualizations have been performed at the angle of attack at which the maximum lift is reached; thus, the fluid is detached at certain regions of the wing. From these images, we can extract that the wing stall is located at the outer flap region of both semi-wings in spite of the asymmetry the propellers should induce as they rotate in the same direction.

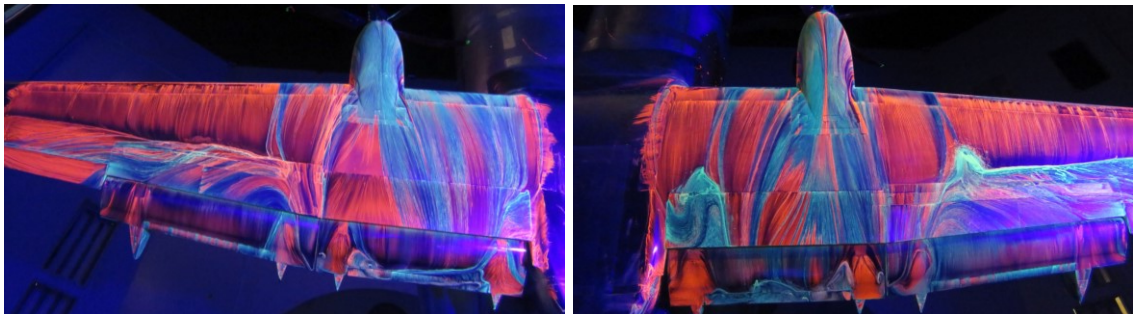

Figure 11 - Wing upper surface (single slotted flap) at CT=0 and maximum lift angle of attack

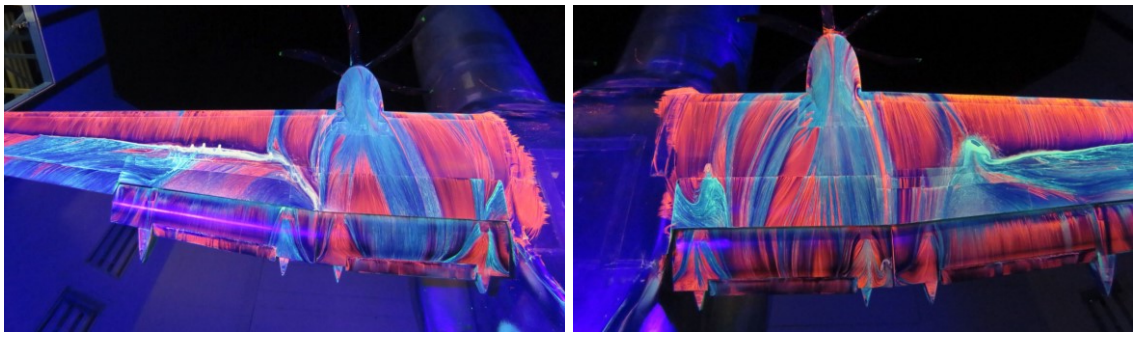

Figure 12 - Wing upper surface (double slotted flap) at CT=0 and maximum lift angle of attack

In addition, it can be observed that the inner flap is partially detached in the trailing edge at single flap while the tab fixes this flow detachment. Note that, the suction appearing at tab leading edge due to the slot causes the flow over the flap remain attached.

The same effect also occurs at high thrust coefficient condition and low angle of attack as it can be observed in Figure 13 and Figure 14.

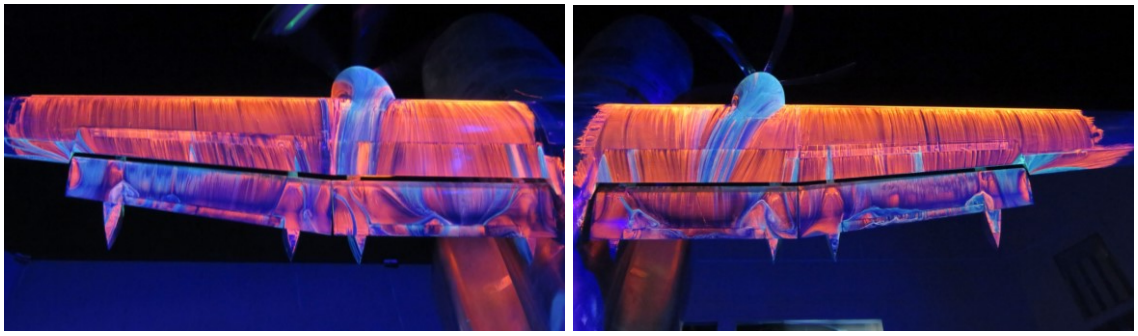

Figure 13 - Wing upper surface (single slotted flap) at high CT and zero angle of attack

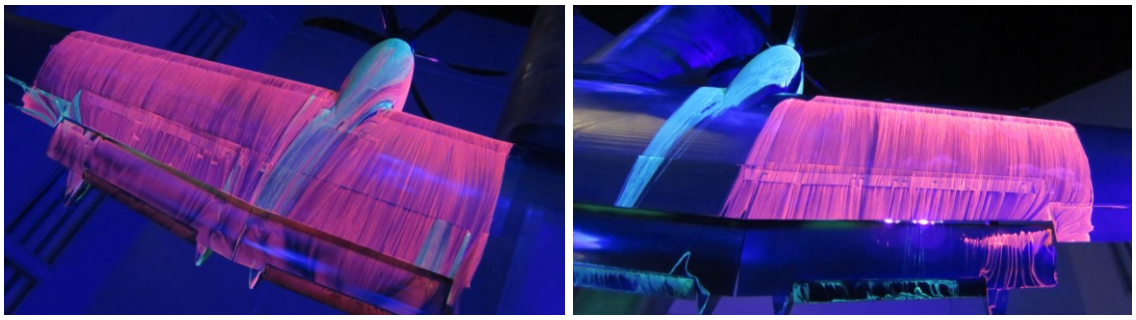

Figure 14 - Wing upper surface (double slotted flap) at high CT and zero angle of attack

5. CFD Results and Comparison with WTT

Through this article we have tried to highlight the importance of the aircraft and propeller interaction and the necessity of correctly predicting those effects since the preliminary design phases. This prediction can be performed by means of Computational Fluid Dynamics (CFD); the assessment of CFD methodologies in order to predict propeller effects is performed in two stages through increasing level of fidelity. Finally, we will compare the CFD results with the wind tunnel results presented in section 4.

5.1 Methodology

The first CFD approach is based on the coupling of the Reynolds Averaged Navier Stokes (RANS) with Blade Element Momentum (BEM) theory. As a first step, this methodology is a simplified view of the problem which looks for a preliminary and fast acquisition of results in order to identify potential risks induced by propeller in the rest of aircraft components.

As any of BEM methods, the propeller blade is discretized in a set of blade span-wise sections from blade root to tip. A sectional database is generated in terms of Reynolds and Mach number dependent polar curves of the airfoils, as well as span-wise chord and twist angle distributions. By specifying number of blades, tilt and toe angles, cyclic pitch and bank angles (depending on the control laws) as wells as the propeller rotational speed and global blade pitch angle, the forces and moments at every section are obtained and coupled with RANS equations through sources terms in the momentum equations. The BEM and RANS interaction methodology has been already introduced by Zori and Rajagopalan [7] and implemented in ANSYS Fluent solver [8].

Once the computations are performed, it is possible to extract axial and tangential velocity components in a predefined set of radial rakes at different azimuthal positions within the propeller plane. According to these velocities, rotational speed, rake position and airfoil polar curves, the span-wise distributions of total velocities, inflow angles, angle of attack, lift and drag, thrust and torque as

well as in-plane forces and moments are obtained. Through the azimuthally dependent in-plane forces and moments distributions, a weighted average is performed to get the 1P forces and moments contribution at every section of the propeller, and finally the global 1P forces and moments of the propeller by direct integration.

Regarding to the CFD model, the mesh is developed as a fully hexahedral multi-block approach with the specific refinements to achieve a correct boundary layer capture by getting a maximum value of y+~1 for the whole wall surfaces group, and raising mesh size up to a minimum of 80 million cells. Respect to the solver, all the CFD simulations were run with ANSYS Fluent solver [9] and [10] (RANS) coupled with Virtual Blade Model (BEM methodology). The air is modeled as an ideal gas with thermodynamic properties temperature dependent and Sutherland's model, and the closure of the problem is performed through the well-known Boussinesq hypotheses (standard RANS turbulence closure approach) through k-ω SST model two equations turbulence model.

The other CFD approach employed is the Lattice Boltzmann Method (L-B) using the PowerFlow solver that has been applied to the configuration with double slotted flap for verification purposes.

L-B emerged as an evolution of the Lattice Gas Cellular Automata [11] to [14] with first approaches from McNamara et al. [15] and [16] and Higuera et al.[17]. LBM have a specific discretization of the Boltzmann equation as reported by He et al.[18]. There are many research teams investigating the compatibility between LBM and the Navier-Stokes equations since the firsts LBM proposals [15] to [17] which is less obvious in compressible regime.

LBM is inherently unsteady which could be taken advantage of for different purposes, like performing very large eddy simulations (VLES) or computing the propeller rotation, among others. Thus, the L-B model includes the true geometry of the propeller blades that rotate during the computation at the prescribed rpm's and blade pitch. The grids in L-B are always Cartesian, representing the "lattice" that makes use of different stencils, depending on the solver, to connect and propagate the physical magnitudes between grid nodes. The adequate grid resolution is achieved by means of grid sub-division in an octree-like manner leading to a few number of grid levels. This way forces the L-B to employ, in one side, immerse boundary methods for the wall boundary conditions and, in another, to make use of wall functions (WF) for modelling the boundary layer. In the case of PowerFLOW, the rotation of the propeller is implemented through a local rotating frame (LRF) which is supported basically in a sliding mesh concept that interpolate magnitudes at the frontier of the rotating disk containing the propeller. PowerFLOW uses a k-ε turbulence model (TM) making specific adaptations on the TM and on the WF to cope with the VLES computations.

The workflow employed (just for the sake of efficiency) with PowerFLOW used two aircraft models that are different only in the grid resolution at the different zones. The less expensive one has about 120M voxels (equivalent to grid elements in RANS) and is computed first to propagate the major convective effects up to obtain a converged solution in terms of forces an moments at the aircraft. The more expensive one has 426M voxels and uses the solution of the former one as initial solution to compute a more detailed and accurate solution at every location.

5.2 Results

A set of power-off and power-on CFD simulations have been performed in order to compare the global coefficients and the 1P loads with the data obtained from wind tunnel tests. Those CFDs have been simulated at wind tunnel Reynolds and Mach numbers for both single and double slotted flaps. Finally, a set of representative images from CFD allow us comparing not only the integral values of both global and 1P coefficients but also the fluid status.

5.2.1 Global Coefficients

Attending the global coefficients it is observed from data obtained via CFD that the RANS simulations provide really accurate results when comparing with wind tunnel results. The power-off lift coefficient estimations at most angles of attack are highly accurate for both flaps as it is shown in Figure 15. On the other hand, while the propeller effect at zero angle of attack is well captured, the lift coefficient derivative is slightly optimistic with RANS methodology while L-B estimations are highly accurate as it can be observed in double slotted flap.

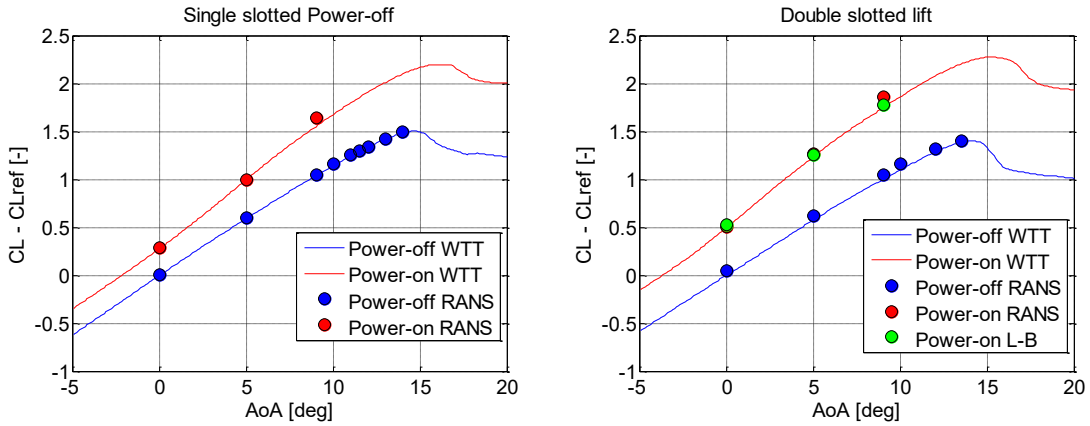

Figure 15 - Lift coefficient CFD vs WTT at power-off (blue), and CT=0.6 (red) for single slotted flap (left) and double slotted flap (right).

Despite the fact the lift coefficient estimations are remarkable; the pitching moment is not as well predicted. The power-off RANS pitching moment deviation from wind tunnel data is almost constant which can be affected by the differences between CFD and wind tunnel geometries. However, the propeller indirect effect on pitch is pessimistic as it is shown in Figure 16. Despite the absolute values are not accurate, the pitching moment derivatives with the angle of attack as well as the loss of aircraft stability due to HTP stall nearness are well captured mainly considering L-B methodology. It is to be noted that, at design phases, it is the aircraft stability which interests the designer; thus, the CFD predictions are really valuable.

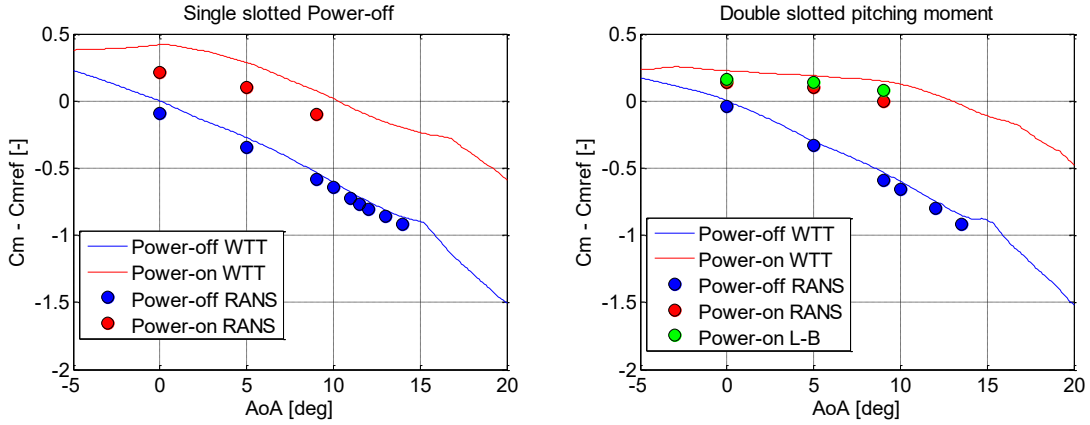

Figure 16 – Pitching moment coefficient CFD vs WTT at power-off (blue), and CT=0.6 (red) for single slotted flap (left) and double slotted flap (right).

Finally, considering the detailed design phase CFD, it is observed that at zero angle of attack and double slotted flap the results are quite similar to those obtained by RANS simulations.

5.2.2 In Plane Loads

In the same way, the global coefficients have been obtained from CFD; it is possible integrating the forces over the propeller blades in Lattice-Boltzmann or estimating the average loads on it as it is described in section 5.1 in the RANS+BEM methodology in order to compare the estimations with the data measured in wind tunnel tests. Let us remember the CZ, CM and CN are those coefficients we have focused on as they are those which mainly depend on the angle of attack.

In Figure 17 the vertical in-plane load obtained by means of CFD is presented. Attending RANS results, estimations represent the wind tunnel test measures. CFD results are in line with wind tunnel data, particularly the force derivative with the angle of attack and the relative trends between both, port and starboard, engines and both flap settings are well captured. In addition the simulation performed with Lattice-Boltzmann is highly accurate.

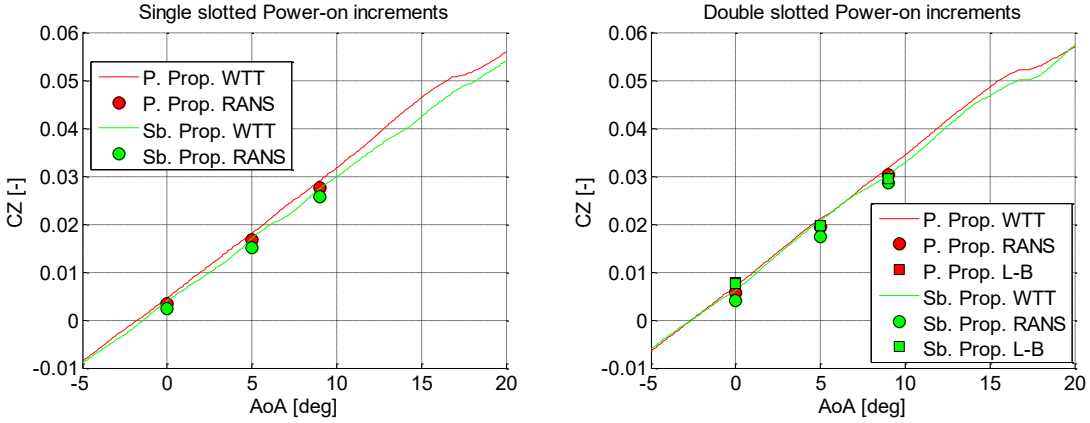

Figure 17 - 1P vertical force, CFD versus WTT, on the port and starboard propellers (CZ). Single slotted flap (left) and double slotted flap (right)

On the other hand, the 1P moment over propeller y-axe (CM) estimations is less accurate as it can be observed in Figure 18. The RANS methodology suggests the CM dependence with the angle of attack is lower than it is extracted from wind tunnel data; however, once again, the relative trends between both propellers and the dependence with the flap setting are coherent. Lattice-Boltzmann simulations slightly improve CFD accuracy in this case.

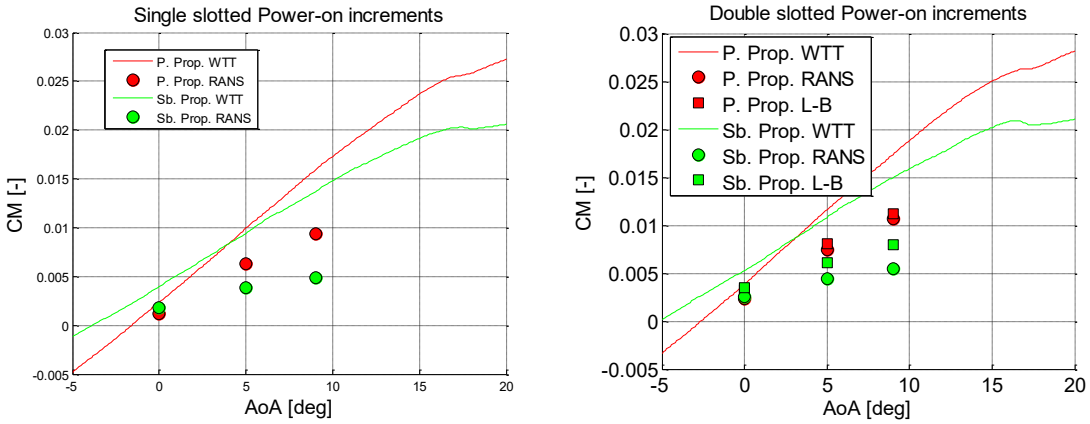

Figure 18 – 1P pitching moment, CFD versus WTT, on the port and starboard propellers (CM). Single slotted flap (left) and double slotted flap (right)

Finally, the CN estimations are much better captured as it is observed in Figure 19. In this case the CFD slightly overpredicts the CN in-plane load, with similar predictions for port and starboard

propellers, whereas wind tunnel gradient CN vs alpha is lower for the port propeller than for the starboard one.

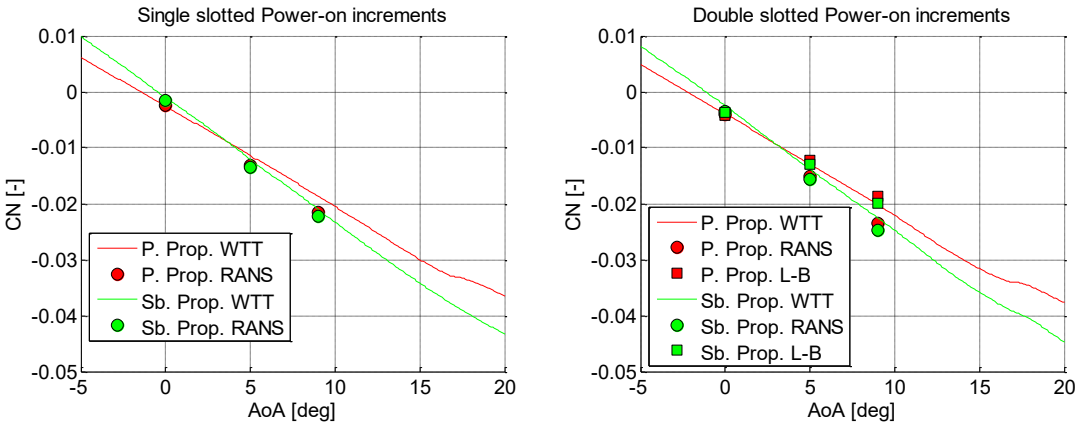

Figure 19 – 1P yawing moment, CFD versus WTT, on the port and starboard propellers (CN). Single slotted flap (left) and double slotted flap (right)

5.2.3 Streamlines on Upper Wing

We are including along this section a set of CFD images obtained by both RANS and L-B methods in order to compare the fluid streamlines with those observed in WTT presented in section 4.2.3.

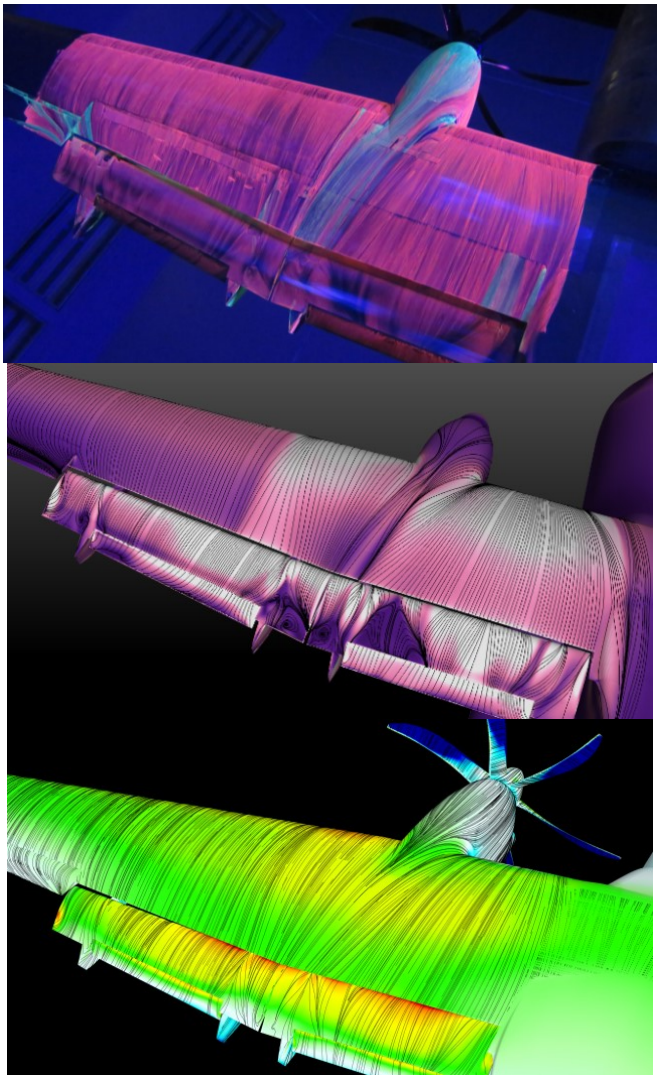

Figure 20 - Wing upper surface (double slotted flap) at high CT and zero angle of attack. Wind Tunnel Test (Upper), RANS CFD (Center) & Lattice Boltzmann CFD (Lower)

In Figure 20, the streamlines over the upper surface of the wing are compared, in this figure, we can observe the accuracy of both CFD methods in the lateral deviation of streamlines from the nacelle, the effect of the flap track faring over the flap and flap-tab surfaces, even the behavior on the aileron and flap joint region.

6. Conclusions

Along this article, the authors have tried to demonstrate and support the necessity of including the propeller effects estimations since preliminary design phases in propeller driven aircrafts. This necessity attends to the great interaction between the propellers and the aircraft performance and stability.

This interaction has been illustrated by means of wind tunnel test measurements and CFD estimations regarding lift and pitching moment coefficient. On one hand the zero angle of attack lift coefficient, its angle of attack derivative and the maximum lift coefficient experiments a great increment due to propeller operation. On the other hand, this lift coefficient affects the angle of attack at tail location which should be considered in the HTP design.

The assessment of CFD methodologies in order to predict propeller effects is performed in two stages through increasing level of fidelity. A RANS+BEM methodology considered in preliminary design phases and a Lattice-Boltzmann methodology for detailed design phase have been presented along the article. Both methodologies have been compared with those results obtained from wind tunnel tests regarding the global coefficients and the propeller in-plane loads.

Finally, we can conclude that both methodologies - with their advantages and drawbacks - are accurate enough to be included within the design cycle of propeller driven aircraft.

7. Acknowledgment

The activities depicted herein have received funding from the European Union's Horizon 2020 research and innovation program, Clean Sky 2 Regional ITD under grant agreement No CSJU-GAM-2014-2015, as part of the design of the Flight Test Bed 2.

8. Contact Author Email Address

Sergio De Lucas-Bodas, mailto: sergio.delucas@airbus.com
David E. Funes-Sebastian, mailto: david.e.funes@airbus.com
Luis P. Ruiz-Calavera, mailto: luis.ruiz@airbus.com
Jorge Narbona-González, mailto: jorge.narbona@airbus.com
Victor Ossorio-Contreras, mailto: victor.ossorio@airbus.com
Juan José Guerra-Crespo, mailto: juan.guerra@airbus.com

9. Copyright Statement

The authors confirm that they, and/or their company or organization, hold copyright on all of the original material included in this paper. The authors also confirm that they have obtained permission, from the copyright holder of any third party material included in this paper, to publish it as part of their paper. The authors confirm that they give permission, or have obtained permission from the copyright holder of this paper, for the publication and distribution of this paper as part of the ICAS proceedings or as individual off-prints from the proceeding

References

[1] Daher. Airbus and Safran team up to develop EcoPulse ™, a distributed hybrid propulsion aircraft demonstrator, Online: https://www.daher.com/en/the-ecopulse-demonstrator-achieves-its-first-key-milestone/

[2] Airbus. *Zeroe*, Online: https://www.airbus.com/innovation/zero-emission/hydrogen/zeroe.html

[3] Dae Kim H. Distributed Propulsion Vehicles. *27th international congress of the aeronautical sciences*. Nice, September 2010.

[4] Stoll A M, Bevirt J, Moore M D, Fredericks W J and Borer N K. Drag Reduction through distributed electric propulsion. *Aviation Technology, Integration, and Operations Conference*, 16-20 June 2014, Atlanta, Georgia

[5] RUAG LWTE, Online: https://www.ruag.ch/en/our-competencies/portfolio/additional-services-products/aerodynamics/aerospace-wind-tunnel-success-based-latest-technology-and-infrastructure

[6] Airbus C295W, Online: https://www.airbus.com/defence/c295.html

[7] Zori L A J and Rajagopalan R G. Navier-Stokes calculation of rotor-airframe interaction in forward flight. *Journal of the American Helicopter Society*, Vol.40, April 1995.

[8] Ruith M. Unstructured, multiplex rotor source model with thrust and moment trimming - Fluent's VBM model. *23rd AIAA Applied Aerodynamics Conference*, Toronto, June 2005.

[9] *ANSYS Fluent Theory Guide Release 15*, ANSYS, Inc., 275 Technology Drive Canonsburg, PA 15317, November 2013.

[10] *ANSYS Fluent User's Guide Release 15,* ANSYS, Inc., 275 Technology Drive Canonsburg, PA 15317, November 2013.

[11] Wolf-Gladrow D A. *Lattice-gas cellular automata and Lattice Boltzmann models: an introduction*. Springer, New York, 2000.

[12] Frisch U, Hasslacher B and Pomeau Y. Lattice-gas automata for the Navier-Stokes equation. *Physical Review Letters*, Vol. 56, No. 14, 1986, pp. 1505–1508. https://doi.org/10.1103/PhysRevLett.56.1505.

[13] Rothman D H, and Zaleski S. *Lattice-gas cellular automata: simple models of complex hydrodynamics*. Cambridge University Press, 1997.

[14] Doolen G D. *Lattice gas methods: theory, applications, and hardware*. MIT Press, Cambridge, Mass, 1991.

[15] McNamara G R and Zanetti G. Use of the Boltzmann equation to simulate lattice-gas automata. *Physical Review Letters*, Vol. 61, No. 20, 1988, pp. 2332–2335. https://doi.org/10.1103/PhysRevLett.61.2332.

[16] Kadanoff L P, McNamara G R and Zanetti G. From automata to fluid flow: comparisons of simulation and theory. *Physical Review A*, Vol. 40, No. 8, 1989, pp. 4527–4541. https://doi.org/10.1103/PhysRevA.40.4527.

[17] Higuera F J and Jiménez J. Boltzmann approach to lattice gas simulations. *Europhysics Letters (EPL)*, Vol. 9, No. 7, 1989, pp. 663–668. https://doi.org/10.1209/0295-5075/9/7/009.

[18] He X and Luo L S. Theory of the Lattice Boltzmann method: from the Boltzmann equation to the Lattice Boltzmann equation. *Physical Review E*, Vol. 56, No. 6, 1997, pp. 6811–6817. https://doi.org/10.1103/PhysRevE.56.6811.